REDUCE GRAPHENE OXIDE NANOSHEETS DERIVED FROM IRAQI *RHHUS CORIARIA*(L.) FRUITS WERE EVALUATED FOR THEIR ANTICANCER AND ANTIBACTERIAL PROPERTIES[a]

EVALUACIÓN DE LAS LÁMINAS DE NANÓXIDO DE GRAFENO REDUCIDO DERIVADAS DE LOS FRUTOS DE *RHUS CORIARIA* (L.) DE IRAK POR SUS PROPIEDADES ANTICANCERÍGENAS Y ANTIBACTERIANAS

AMENAH SALIM KADHIM[b], ZAINAB SHAKIR ABDULLAH AL-ALI[c][*]

ABSTRACT: In this study, reduced graphene oxide nanosheets (rGO) were biosynthesized using the methanolic extract of Iraqi *Rhus coriaria* (L.) fruits with substantial bioreduction capabilities. The GC-MS analysis of the methanolic extract of Iraqi *Rhus coriaria* (L.) fruits was used to determine the synthesis mechanism of rGO nanosheets. The synthesized graphene oxide (GO) and the biosynthesized methanolic extract of Iraqi *Rhus coriaria* (L.) fruits-rGO nanosheets (MERCF-rGO) were characterized using UV-Vis at 226 nm, and 238 nm, respectively. FTIR explained the functional groups of GO and MERCF-rGO nanosheets, XRD spectra of the GO and MERCF-rGO show the sizes at 10.42 nm, and 4.07 nm, TEM observed the size of GO and MERCF-rGO at 15.54 nm and 9.6 nm. As well as FESEM of GO and MERCF-rGO was carried out to explain sheet shape about them. Raman spectroscopy of GO and MERCF-rGO displayed the two peaks D at (1353 cm^{-1}, 1336 cm^{-1}) and G at (1597 cm^{-1}, 1594 cm^{-1}) respectively. MERCF-rGO nanosheets showed activity against antibacterial gram-positive (*Staphylococcus aureus*) and gram-negative (*Escherichia coli*), cytotoxicity by MTT assay against breast cancer MCF-7 cell line IC$_{50}$ at 251.99 μg/mL, genotoxicity fragmented DNA of MCF-7 by comet assay. Comprehensively, the green synthesis of rGO is safe, the lowest cost and developable biogenic nano-formulation of Iraqi *Rhus coriaria* (L.)–rGO owns antibacterial and anticancer therapeutic applications.
KEYWORDS: Iraqi *Rhus coriaria* (L.); MCF-7 breast cancer; mechanism of bioreduction rGO; reduced graphene oxide (rGO). Characterization; bricks; mechanical

RESUMEN: En este estudio, se biosintetizaron nanohojas de óxido de grafeno reducido (rGO) utilizando el extracto metanólico de frutos iraquíes de *Rhus coriaria* (L.) con importantes capacidades de biorreducción. El análisis GC-MS del extracto metanólico de los frutos iraquíes de *Rhus coriaria* (L.) se utilizó para determinar el mecanismo de síntesis de las nanohojas de rGO. El óxido de grafeno sintetizado (GO) y el extracto metanólico biosintetizado de nanohojas

[b]Department of Chemistry, College of Science, University of Thi Qar,64001,Iraq.
[c]Department of Chemistry, College of Science, University of Basrah, 61004, Iraq
[*]Correspondence author: zainab.abdulah@uobasrah.edu.iq

de frutos-rGO de *Rhus coriaria* (L.) iraquí (MERCF-rGO) se caracterizaron utilizando UV-Vis a 226 nm y 238 nm, respectivamente. FTIR explicó los grupos funcionales de las nanohojas GO y MERCF-rGO, los espectros XRD de GO y MERCF-rGO muestran los tamaños a 10,42 nm y 4,07 nm, TEM observó el tamaño de GO y MERCF-rGO a 15,54 nm y 9,6 nm. Además, se llevó a cabo FESEM de GO y MERCF-rGO para explicar la forma de las hojas. La espectroscopia Raman de GO y MERCF-rGO mostró los dos picos D en ($1353\ cm^{-1}$, $1336\ cm^{-1}$) y G en ($1597\ cm^{-1}$, $1594\ cm^{-1}$) respectivamente. Las nanohojas MERCF-rGO mostraron actividad contra antibacterianos grampositivos (*Staphylococcus aureus*) y gramnegativos (*Escherichia coli*), citotoxicidad mediante ensayo MTT contra cáncer de mama, línea celular MCF-7 IC_{50} a 251,99 μg/mL, genotoxicidad ADN fragmentado de MCF-7 por ensayo de cometa. En términos generales, la síntesis verde de rGO es segura, la nanoformulación biogénica desarrollable y de menor costo de *Rhus coriaria* (L.) iraquí; rGO posee aplicaciones terapéuticas antibacterianas y anticancerígenas.

PALABRAS CLAVE: *Rhus coriaria* iraquí (L.); cáncer de mama MCF-7; mecanismo de biorreducción rGO; óxido de grafeno reducido (rGO).

1. INTRODUCTION

The reduced graphene oxide (rGO) is one of many graphene derivatives with a hexagonal structure similar to graphene but with few oxygen functional groups. This material has several properties, including a large surface, enhanced electrical conductivity, excellent optical adsorption, and a hydrophobic nature. Recently, eco-friendly strategies for preparing reduced graphene oxide (rGO) have become one of science's most widely discussed areas (Al-Abboodi *et al.*, 2017; Yi *et al.*, 2020). Chemical, thermal, and biological reduction methods can synthesize rGO. Chemical reduction uses reduce hazardous agents such as $NaBH_4$, hydrazine, and hydroquinone. Moreover the final product also had toxic materials, expensive methods, and impurities (Cheng *et al.*, 2017). Reducing graphene oxide with thermal reduction uses heat. Known as (thermal annealing reduction), it takes place in a vacuum, is inert, and is carried out at high temperatures. As a result, it is not favored over the other methods (Jiříčková *et al.*, 2022)). The biological reduction method of rGO (green synthesis) is preferred over chemical and thermal reduction methods. Natural reducing agents are used, either microbes or plants, and it is a non-toxic, low-cost, eco-friendly, safe, and grants a higher effect than any other rGO synthesis methods (Mahmoud, 2020). The bioreduction (green) method became more significant and gained the attention of researchers as a result (Lingaraju *et al.*, 2019). A green synthesis method for rGO can be used in many biomedical applications, such as anticancer therapies (Choi *et al.*, 2018), antimicrobial activities (Rani *et al.*, 2017), cell image and drug delivery (Wu *et al.*, 2012). As a microcarrier for DOX load, riboflavin-rGO is made from the reduction of GO by riboflavin as a reducing agent (Ma *et al.*, 2015). rGO derived from the reduction of GO by *Euphorbia milii* plant extract, which used as a carrier for the cancer drug paclitaxel (Lin *et al.*, 2019). rGO is used in chemotherapy and is a dual drug for cell killing, such as rGO is functionalized by polymer PF-127, as a carrier for *Curcumin* extract, and Paclitaxel has shown anti-tumor efficacy in both A549 lung cancer cells and MDA-MB-231 breast cancer cells (Muthoosamy *et al.*, 2016). Recent studies showed phytochemicals biomolecules extracted from plants such as *Jasminum sambac* (L.) *Aiton* leaves are considered interesting biosources in the medical field and play an essential role in the bioreduction of silver and gold nanoparticles (Bidan & Al-Ali, 2022; Bidan &
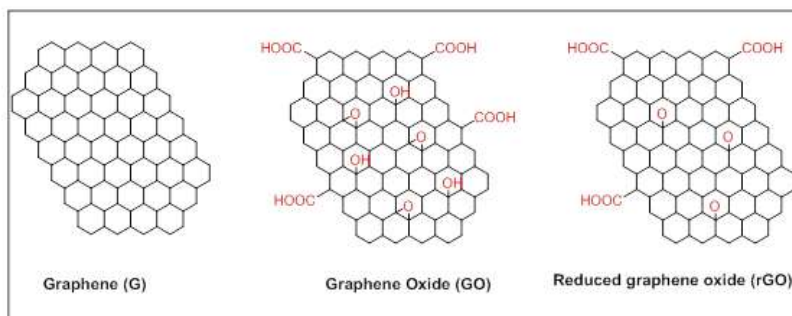
Figure 1: The structures of graphene (G), graphene oxide (GO), and reduced graphene oxide (rGO). Source: Elaborated by the authors.

Al-Ali, 2023), see Fig. 1.

This study aimed to characterize the phytochemical structures' role in rGO biosynthesis by GC/MS analysis of *Rhus coriaria* (L.) fruit cultured in Iraq. There is no report about using Iraqi *Rhus coriaria* (L.) fruit extract as a green reducing agent to reduce GO. Consequently, the variation in composite structures of Iraqi *Rhus coriaria* (L.) is related to geographical district, harvesting time, environmental effects (soil, climate), genetic differences, extraction method, and analytical routes (Giovanelli. *et al.*, 2017). This study discusses the proposed synthesis mechanism of biosynthesized rGO from *Rhus coriaria* (L.) and *Rhus coriaria-rGO* properties as antibacterial and anticancer.

2. EXPERIMENTAL SECTION

2.1. Preparation of graphene oxide (GO)

The improved Hummer method was used for GO synthesis (Marcano *et al.*, 2010). 3g of graphite powder was added to the mixture of 360 mL of concentrated sulfuric acid (H_2SO_4) (18.4 M) and 40 mL of phosphoric acid (H_3PO_4) (15.18 M) in a ratio of 9:1 with a stirrer, then 18 g of potassium permanganate ($KMnO_4$) was slowly added to the previous mixture with continuous stirrer until a deep green color solution was obtained. The reaction mixture was placed in an ice bath with salt and monitored using a thermometer to maintain a temperature of 50 °C and stirred for 12 h. The reaction was cooled to room temperature and poured on 400 mL of ice with 3 mL of 30 % hydrogen peroxide (H_2O_2). The formed solution was yellow. It was then sifted through a sieve, filtered throug a sieve and filtered through the polyester fabric. A sieve is placed on top of a polyester cloth; the mixture is poured into the sieve; the mixture is filtered through the sieve; then the polyester cloth is used to form a soft and easy fabric known as (Mellmal). A fter that, the filtrate was centrifuged (4000 rpm for 4 h) while the supernatant decanted away, and the precipitating material was washed in 200 mL of water, 200 mL of 30 % hydrochloric acid (HCl) and 200 mL of ethanol (C_2H_5OH) (two times the process was repeated). The product was collected, coagulated with 200 mL of ether (($C_2H_5)_2O$) and filtered through Whatman filter paper No.1. The product obtained on the filter was

vacuum-dried overnight at room temperature.

2.2. Plant material

The fresh fruits of *Rhus coriaria* (L.) were collected from Chamchamal City in Sulaymaniyah governorate in Iraq in August 2021. This plant belongs to the *Anacardiaceae* family. The fruits separated from other plant residues and fruits were washed with water two times to remove the dust, then repeated the washing step twice by using deionized water (DI) until it confirmed that there were no contaminants; followed these fruits leave it to dry under the following conditions away from light at room temperature for 3 days. The dried fruits were ground to fine powder by a blender and then in a closed container at 4°C until used.

2.3. Preparation of methanolic extract *Rhus coriaria* (L.) fruits (MERCF-rGO)

Methanolic extract of *Rhus coriaria* (L.) fruits (MERCF) was prepared following a modified procedure (Mazaheri *et al.*, 2017). Ten g of fruits powder of *Rhus coriaria* (L.) was blended with 100 mL of 70% methanol (CH_3OH) and stirred at 40 °C for 30 min, cooled and filtered the solution by using a Büchner funnel that separated the extract from the solid material. The filter was combined and used a rotary evaporator at 40 ° Cuntil dryness. The dry powder (extract) is stored until use.

2.4. Biosynthesized of rGO nanosheets (MERCF-rGO)

Reduced graphene oxide (MERCF-rGO) has been synthesized from methanolic extract of *Rhus coriaria* (L.) fruits following a procedure published by (Thiyagarajulu *et al.*, 2020). Graphene oxide (GO) 0.04 g is dissolved in 100 mL distilled water. The GO solution is added to 0.01 g of dried methanolic extract of *Rhus coriaria* (L.) fruits, to produce a yellowish–brown reaction mixture. Then, the reaction mixture is sonicated for 40 min. The yellowish–brown GO solution was refluxed at 95 °C in a water bath for 12 h. After that, the GO's yellowish–brown color converted to black, evidence of success in removing oxygen groups of GO. The yellowish-brown color of the reaction mixture then turned black, indictating that oxygen groups were successfully removed from GO. The black color mixture was centrifuged at 10000 rpm for 10 min, and the precipitate was washed with deionized water (DI) and vaccuumed to obtain good, dried MERCF–rGO. The biosynthesized MERCF-rGO was stored in a vial for further studies of characterization and biomedical applications.

2.5. Characterization techniques of GO and MERCF-rGO

The GO and the biosynthesis of MERCF-rGO were characterized through the following instruments UV-visible spectroscopy (Shimadzu, UV–1900), Fourier-transform infrared spectroscopy (FTIR) recorded the wavelength range of (4000-400 cm^{-1}) (Shimadzu, IRAffinity-1800), X-ray diffraction by (PHILIPS, PW 1730) with Cu-Kα radiation ($\lambda = 0.1540$ nm). Raman spectroscopy (TESCAN, N1–541). To evaluate the surface morphology of the samples by Field emission scanning electronic microscopic (FESEM) (TESCAN,

MIRA III) and Transmission electron microscopy (TEM) (Car-Zeiss, EM10C-100 KV). GC/MS analysis (Agilent 7820A / USA) was used to detect the phytochemicals of *Rhus coriaria* (L.) fruits.

2.6. Antibacterial activity of MERCF-rGO

The antibacterial activity was investigated against *Staphylococcus aureus* (*S. aureus*) and *Escherichia coli* (*E. coli*) using an agar well diffusion approach following a procedure with a slight modification (Mahendran *et al.*, 2016). About 20 mL of Muller–Hinton (MH) agar was aseptically poured into sterile Petri dishes. The bacterial species were collected using a sterile wire loop from their stock cultures. After culturing the organisms, 6 mm–diameter wells were bored on the agar plates using a sterile tip. 50 μL for different MERCF-rGO concentrations was added to the bored wells. MERCF-rGO concentrations were used (15.62 μg/mL, 31.25 μg/mL, 62.5 μg/mL and 125 μg/mL) each concentration was assayed with both against *S. aureus* and *E. coli*. Also, the antibacterial activity was investigated with the commercial antibiotics (Ciprofloxacin, Augmentin, and Cefuroxime) using the same concentrations of MERCF-rGO and a further concentration of 250 μg/mL. The samples were dissolved in distilled water (DW) and the test microorganisms were incubated overnight at 37 °C before measuring and recording the zones of inhibition diameter in mm.

2.7. Cytotoxicity of MERCF-rGO (MTT assay)

The cell viability was performed by an MTT assay, which is one of the colorimetric assays of the viable cells, considered the simplest of them, that works on reducing MTT (3-(4,5-dimethyl thiazol-2-yl)-2,5-diphenyltetrazolium bromide) (yellow colored tetrazolium salt, soluble in water) to Formazan crystals (purple colored, insoluble in water) in live cell mitochondria. MCF-7 cells were purchased from the Iranian Biological Resource Center (Tehran, Iran) and were maintained in RPMI-1640 (Capricorn, Germany) supplemented with 10 % Fetal bovine serum (FBS), 100 units/mL penicillin and 100 μg/mL *streptomycin*. Cells were passaged using Trypsin-EDTA, reseeded at 80 % confluence twice a week, and incubated at 37 °C , the MERCF-rGO cytotoxicity was determined during the MTT assay (Punniyakotti et al., 2021), with some modifications. The cell line (MCF-7) was cultured at 96-well plate at a 1×10^5 cell/well for 24 h at optimal conditions (37°C, 5 % CO_2 in a humidified incubator). Next, the growth media (10 % FBS) was removed, and the cells were washed two times with phosphate-buffered saline (PBS). New maintenance RPMI medium (10 % FBS) containing (12.5, 25, 50, 100 and 200 μg/mL) of MERCF-rGO was added, and the cells were incubated for 72 h. Triple wells were analyzed for each concentration, and column elution buffer was used as the control. A 10 μL solution of freshly prepared 5 mg/mL MTT in PBS was added to each well and incubated for 4 h. The media was removed, and DMSO was added at 100 μL/well. Plates were shaken gently to facilitate formazan crystal solubilization. The absorbance was measured at 545 nm using a microplate reader (Gennex Lab, USA). The control group's mean optical absorbance was set to 100 %, and the optical absorbance of the other examinational groups was calculated as a percentage of the control group's value. The percentages of cell toxicity and half-maximal inhibitory concentration (IC$_{50}$)

were calculated.

2.8. Single-cell gel electrophoresis (SCGE)

DNA damage was evaluated using the alkaline comet assay (Hinzmann *et al.*, 2014) with some modifications. MCF-7 cell line was cultured in 25 cm^2 flasks for 24 h (37°C, 5% CO$_2$). Afterward, they were treated with agent methanol extracted from MERCF-rGO at IC$_{50}$ concentration (251.99 μg/mL) for 48 h (37°C, 5% CO$_2$). Cells were trypsinized, then centrifuged (1000 rpm, 5 min) in fresh culture medium and rinsed twice with Mg$^-$ and Ca-free ice-cold PBS and centrifuged (1000 rpm, 5 min). The cells (1x10^4) were treated with low melting point agarose (type VII) and transferred onto a glass slide pre-coated with high melting point agarose (type I). Then, the slides were placed in a lysis solution (2.5 M NaCl, 100 mM EDTA, 10 mM Tris base, 1% Triton X–100, pH 10) at 4°C for 60 min. After lysis of the cells in the solidified agarose, DNA was unwound by alkaline treatment. Afterwards, the slides were rinsed in electrophoresis buffer (TBE) (300 mM NaOH and 1 mM EDTA, pH > 13) for 30 min at 4°C. Then, electrophoresis was carried out at a voltage of 1.0 V cm^{-1}, 490 mA intensity for 20 min at 4°C. Staining was carried out with the EtBr (0.5 μg/mL) method. In this assay, the migration distance of DNA measures the amount of DNA damage under a certain condition. After electrophoresis, comet slides were washed in 0.4 M Tris–HCl (pH 7.5) and fixed for 10 min in absolute alcohol. One hundred nuclei were counted on each slide and a percentage of cells with damaged and non-damaged DNA was obtained. In the count, the cells were divided into two categories: undamaged DNA and damaged DNA. A fluorescence microscope was used to photograph the DNA damage (BX53 Olympus, Germany). According to tail size, it is divided into the following five classes: class 1- no tail; class 2– tail shorter than the diameter of the head (nucleus); class 3– tail length 1-2 times the diameter of the head; class 4– tail length more than twice the diameter of the head; class 5- no head with maximal damage.

3. RESULTS AND DISCUSSION

3.1. UV-vis spectroscopy

The reduced graphene oxide by methanolic extract of Iraqi *Rhus coriaria* (L.) fruits (MERCF-rGO) was observed by UV-visible spectra that showed the peak at 238 nm. Also, this peak represented the redshift to the absorbance peak in GO spectra, which showed the peak at 226 nm, it was indicated to $\pi - \pi^*$ transition, and the two peaks in GO spectra is a weak peak at 296 nm, which represents n–π^* transition (Olumurewa *et al.*, 2017). The graphite spectra showed a weak peak at 282 nm that induced the $\pi - \pi^*$ electronic transition of the $C = C$ bonds. Furthermore, the redshift is explained by the replacement of oxygen functional groups by the $C = C$ bonds and the extending sp^2 hybridization in the carbon network. The results showed the UV-vis spectra of rGO that compared with the UV-vis spectra of GO, which displayed the redshift from the absorbance peak at 226 nm of GO to 238 nm of rGO respectively, the redshift peak in the spectrum of rGO confirmed the reduction of GO to rGO. The transition from brown to black provides this Fig. 2.
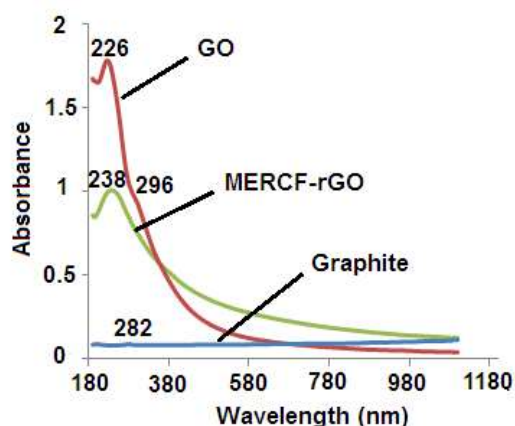
REDUCE GRAPHENE OXIDE NANOSHEETS DERIVED FROM IRAQI *RHHUS CORIARIA*(L.) FRUITS WERE EVALUATED FOR THEIR ANTICANCER AND ANTIBACTERIAL

PROPERTIES

Figure 2: UV-vis spectroscopy of Graphite, GO and MERCF-rGO.

3.2. FTIR analysis

FTIR spectroscopic to characterize potential functional groups of graphite, GO, and MERCF-rGO to compare them and confirm the reduction of GO to rGO by methanolic extract of *Rhus coriaria* (L.) fruits. The FTIR spectrum of graphite appeared to peak at 1639 cm^{-1} ($C = C$), which indicated the stretching vibration of the double bond and formed the carbon structure of graphite. Where the FTIR spectra of GO observed peaks at 3360 and 1454 cm^{-1}, these peaks were due to the stretching vibration and bending vibration of the hydroxyl groups ($O - H$), respectively which attributed to the water molecules adsorbed on the surface of GO; this confirms the hydrophilic natural of GO. Moreover, the spectrum showed bonds the peaks at 2920, 2850, 1739, 1620, 1222, and 1053 cm^{-1}, which are attributed to the stretching vibration of aliphatic ($C - H$), carbonyl groups stretching ($C = O$) of carboxyl ($COOH$), carbon-carbon double bond stretching ($C = C$). Finally, the stretching of epoxy and alkoxy ($C - O$), respectively (Rochman *et al.*, 2019). After the reduction process by methanolic extract of Iraqi *Rhus coriaria* (L.) fruits. The FTIR spectra of MERCF-rGO showed peaks at 3309, 1419 cm^{-1}, representing the stretching vibration and binding vibration of hydroxyl groups ($O - H$). These peaks were lower intensity than the peaks of hydroxyl groups in GO spectra. The peak at 1643 cm^{-1} represented carbon–carbon double bond stretching ($C = C$) increased by comparison with the same peak in GO spectra Fig. 3. The FTIR spectra of rGO compared with the FTIR spectra of GO proved some of the removed peaks. They decreased from the rGO spectra as the stretching vibration peak of the $C = C$ band increased by comparison with the same peak in GO spectra. Also, the peaks disappeared in the FTIR spectra of MERCF-rGO by comparison with GO spectra as a peak at 1739 cm−1; this confirmed the formation of rGO (Khan *et al.*, 2015). This induced the successful reduction of GO by *Rhus coriaria* (L.) fruits.
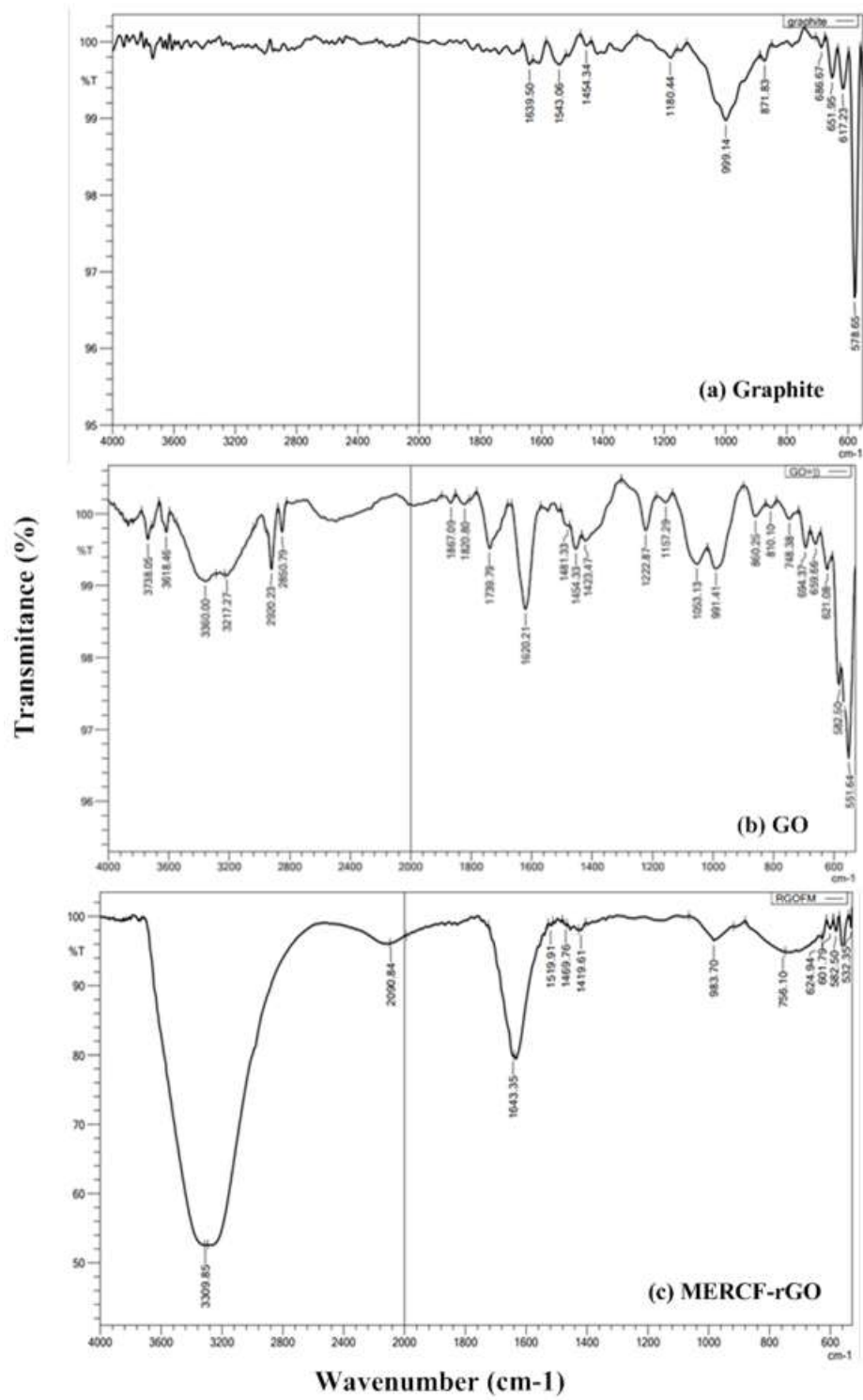
Figure 3: UV-vis spectroscopy of Graphite, GO and MERCF-rGO.

Table 1: XRD data of graphite, GO, MERCF-rGO.

Samples	2θ	FWHM	d-spacing (nm)	Crystal size (nm)
Graphite	26.68	0.2952	0.334025	28.90
GO	11.42	0.8004	0.789564	10.42
MERCF-rGO	22.31	1.9680	0.398459	4.076

3.3. X-ray diffraction analysis (XRD)

XRD is used to know the changes in the crystal structure of graphite, GO and MERCF-rGO. Fig. 4 shows the XRD of graphite, which explains the high intensity and sharp peak at $2\theta = 26.68°$, including the interlayer spacing of 0.334 nm. It also, shows the typical X-ray diffraction structure of GO, which clearly showed the presence of a broad and high-intensity peck at $2\theta = 11.42°$ with a layer spacing of 0.789 nm. The XRD of MERCF-rGO explained the two peaks: one peak at $2\theta = 10.99$ (d-spacing 0.804 nm), and two peak was broad at $2\theta = 22.31°$ (d-spacing 0.398 nm). The crystallite size of the samples was calculated through *Scherrer's* equation in Eq. 1, as shown in Table 1. The XRD spectra results of graphite, GO, and rGO showed a strong peak of graphite, which agrees with the search (Emiru & Ayele, 2017). Whereas the peak shifted to a lower angle of GO, this peak was larger than the peak for graphite. The value of the distance between layers indicates the separation of the layers from each other. The measurement also shows the presence of some peaks of low intensity, which may be attributed to the presence of unoxidized graphite residues, although their percentage is considered negligible. The disappearance of the band at about $26°$ that appears in the graphite is further evidence of the formation of graphene oxide with very high purity (Chandu *et al.*, 2017). In contrast, the results of XRD spectra of rGO appeared in two peaks, the high and low peaks. The d-spacing for two peaks of MERCF-rGO was decreased compared with the d-spacing of GO due to the removal of the functional groups of oxygen where the high peak was the value closed from the peak value graphene.

$$D = \frac{K\lambda}{\beta \cos(\theta)} \tag{1}$$

Where: D = Crystal size , K = Constant equal 0.9 , $\lambda = Wavelength$ (0.154 nm) , β = FWHM in radians
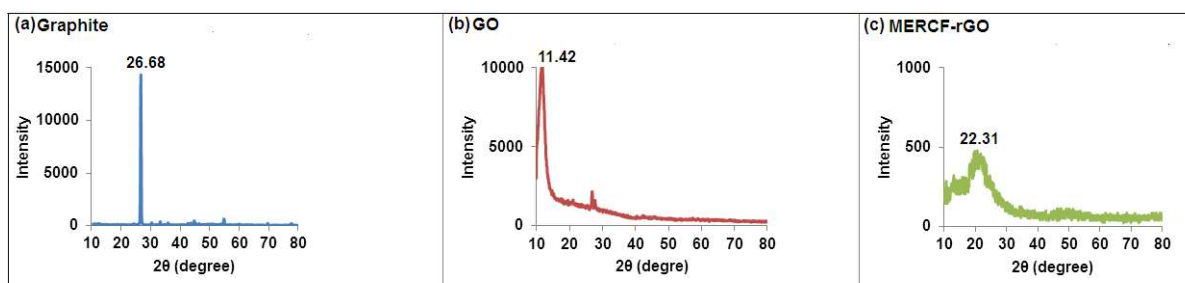

Figure 4: XRD patterns of (a) Graphite, (b) GO and (c) MERCF-rGO.

3.4. Raman spectroscopy

Raman spectroscopy is a powerful technique employed widely for identifying the structure of graphene-related materials, which explains the two peaks: the D and G peaks. The D peak is connected with the breathing mode of Kaba point phonons of (A1g symmetry). The surface defects of graphene represent this, while the G peak is indicated as the first order of E_{2g} phonons for the sp^2 hybridized carbon atoms (Chu $et\ al.$, 2014). The Raman spectra of graphite, GO, and MERCF-rGO showed the presence of the two high-intensity lines for graphite; the first appeared at 1576 cm^{-1}, which is attributed to the G band, and the second was at 2688 cm^{-1}, which indicated the 2D band. Moreover, the measurement showed the line presence of low intensity at 1330 cm^{-1}, representing D band (Alhwaige $et\ al.$, 2015). In contrast, the Raman spectra of the synthesized GO by the oxidation process explained the two bonds, the D and G bands, at 1353 cm^{-1} and 1597 cm^{-1}, respectively. The Raman spectra of MERCF-rGO showed both D and G bands at 1336 cm^{-1} and 1594 cm^{-1}. The value of the intensity ratio (I_D/I_G) of GO and MERCF-rGO was determined to be 0.84 and 1.02, respectively; see Fig. 5. The Raman spectra results of graphite, GO and MERCF-rGO, after the comparison between GO and graphite noticed the G band was widened and the blue-shifted toward the higher wavenumber in GO while the G band in graphite was sharped and the lower wavenumber. Furthermore, the D band of the GO was distinguished. This provided the disintegration of the in-plane sp^2 domain in GO because of the extensive oxidative process (Kim $et\ al.$, 2013). The value (I_D/I_G) is increased of MERCF-rGO compared with that of GO. The high ratio of GO indicated the occurrence of oxidation on the hybrid bonds with sp^2. On the other hand, the high ratio of MERCF-rGO explained the disorder of the graphene sheets. These results agree with the previously reported Raman spectra findings of rGO attained by the reduction of GO using another nature-reducing agent as rose water (Haghighi & Tabrizi , 2013).

3.5. Field emission scanning electron microscope (FESEM)

It is used to study the morphology of GO and MERCF-rGO. The image of the surface of GO is the structure of folded sheets with wrinkled surfaces, and its morphology looked like a waverly carpet when the measurement zoomed to a small nanoscale that showed a thickness in the range (14.11 nm–30.59 nm), whereas the surface of MERCF-rGO sheets explained thin layers, coarse and wave surfaces with thickness at the range between (33.8 nm–54.7 nm), as shown in Fig. 6. FESEM images showed wrinkled and folded regions. On the other hand, the FESEM image of MERCF-rGO was explained upon comparison with the morphology of GO owing to the removal of some wrinkles and folds, where the sheets become more accessible to move due to the intercalation of the oxygen functional groups through the oxidation process (Aunkor $et\ al.$, 2015). The morphology of GO and MERCF-rGO were sheet-like structures, which induced the successful reduction of GO to rGO using the methanol extract of $Rhus\ coriaria$ (L.) fruits.

3.6. Transmission electron microscopy (TEM)

A TEM instrument is used to determine particle size, shape, and morphology. TEM images of the prepared GO explained very clear sheet-like structures, the measurement also proved the sheets were not aggregated
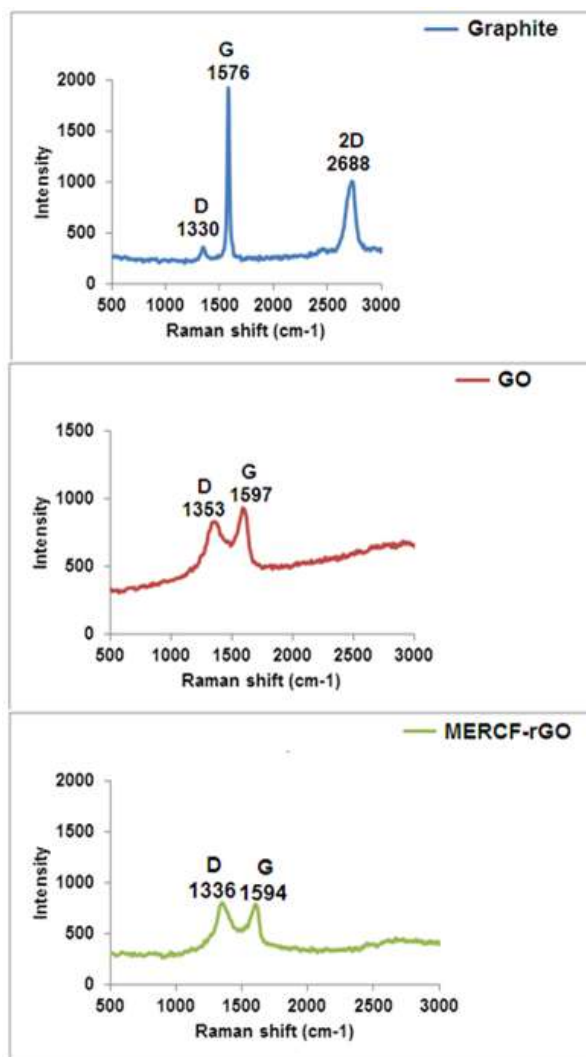
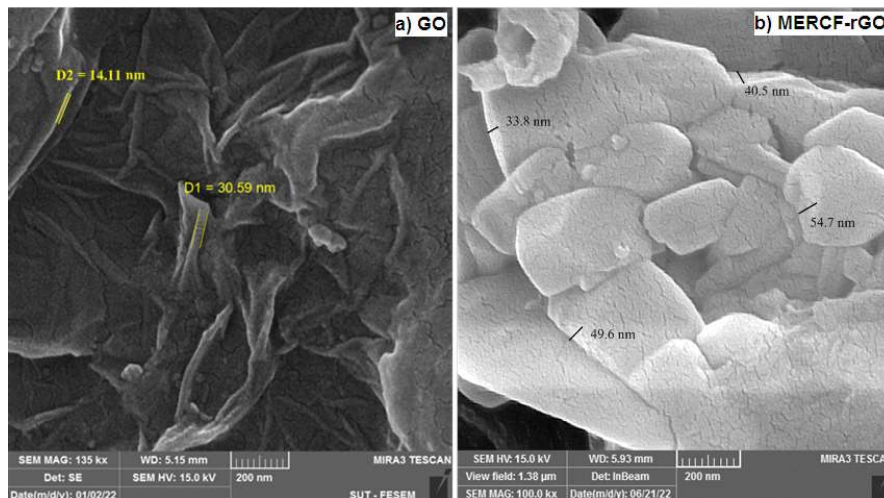Figure 5: Raman spectra of graphite, GO and MERCF-rGO.

Figure 6: FESEM images of (a) GO and (b) MERCF-rGO

with more than three sheets, which proves the formation of few–layered graphene oxide, also indicates the few layers of GO (transparent region), while multilayer of GO (dark region) when the measurement is zoomed that explained the wrinkled surface and size 15.54 nm. In contrast, the TEM image of MERCF-rGO observed the sheet structure with different layers of graphene with dimensions. That do not exceed 9.6 nm also, the MERCF-rGO sheet displayed natural silk, wrinkled surface and corrugation on the edges of the layer, Fig. 7 . TEM image of MERCF-rGO appeared the corrugations on the edge of the carbon layer are similar to the previous reports (Zhu *et al.*, 2010). The dark areas explained the thick stacking nanostructure of many GO and MERCF-rGO layers. The lower opaque areas designate much thinner sheets of GO and MERCF-rGO layers, indicating their delamination. This exfoliation might increase the surface area of the synthesized materials.

3.7.   GC/MS analysis of a methanolic extract of Iraqi *Rhus coriaria* (L.) fruits

The methanolic extract Iraqi *Rhus coriaria* (L.) fruit (MERCF) was analyzed by GC/MS spectra. In this sample was identified 25 compounds as shown Fig. 8 , which included the different classifications of compounds such as essential oils esters (59.25 %) followed by essential oils (31.46 %), polyphenols (2.69 %), alcohols (1.26 %), cyclic amide (1.89 %), ketones (0.86 %), aldehydes(1.05 %), amines (0.85 %), and ethers (0.71 %) as shown in Table 2.

Essential oils esters: The major component of this class was 9-octadecenoic acid, methyl ester (E) (19.76 %); 9,12-octadecadienoic acid, methyl ester (14.58 %); hexadecanoic acid, methyl ester (8.72 %); 11-octadecenoic acid, methyl ester (7.81 %); 8,11-octadecadienoic acid, methyl ester (3.99 %); acetic acid, hydroxyl, ethyl ester (1.86 %); isopropyl linoleate (1.18 %); ethyl formate (0.83 %) and eicosanoic acid, methyl ester (0.52 %). Essential oils: which presented a high percentage after the essential oils esters: *cis*–
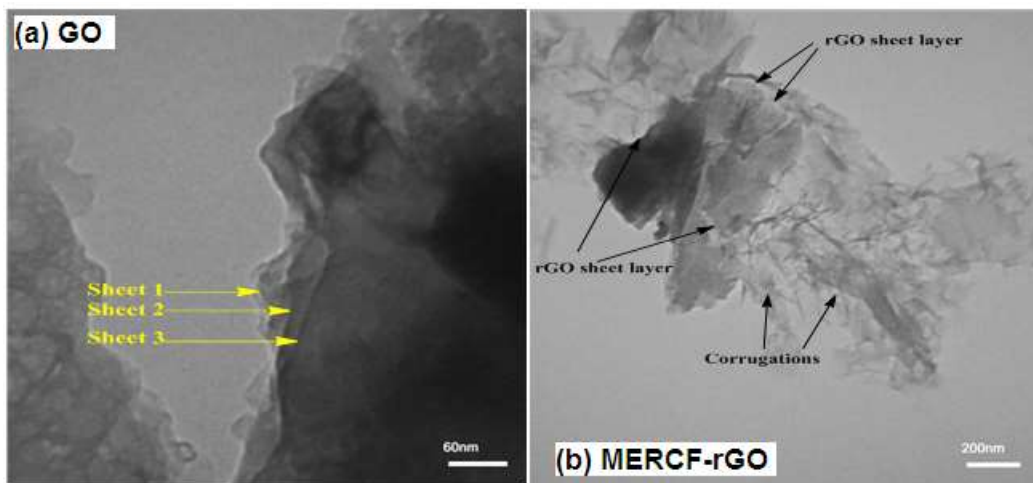
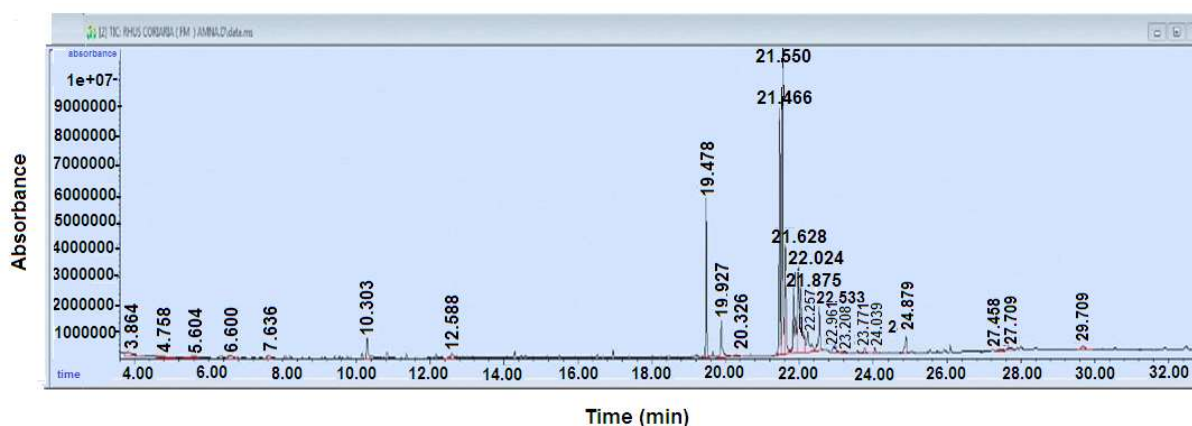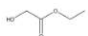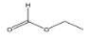Figure 7: TEM images of (a) GO and (b) MERCF-rGO
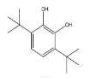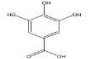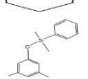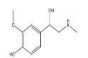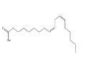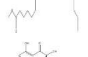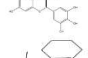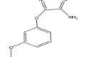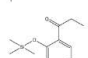
Figure 8: TEM images of (a) GO and (b) MERCF-rGO

13–octadecenoic acid, (15.63 %); 9,12-octadecadienoic acid (Z,Z) (7.78 %); n-hexadecanoic acid (3.7 %); cis-vaccenic acid (3.69 %) and oleic acid (0.66 %). Polyphenols: these include the large groups of compounds such as phenolic acid, flavonoid etc., Myricetin (1.55 %); metanephrine (0.6 %) and Gallic acid (0.54 %). Alcohols: 1,2-benzene-3,5-bis(1,1-dimethylethyl) (0.77 %) and 1-propanol (0.49 %). Ketones: propiophenone-2-trimethoxy (0.86 %). Cyclic amides: caprolactam (1.89 %). Aldehydes: Cyclobarbital (0.55 %); cis-11-hexadecenal (0.50 %). Amines: 1,2,5-oxadiazol-3-amine-4(3-methoxy) (0.85 %). Ethers: Benzen,1-[2-(2-chloroethoxy) ethoxy]-4-(1,1,3,3-tetramethyl butyl) (0.71 %).

Methanolic extract of Iraqi *Rhus coriaria* (L.) fruits (MERCF) contains the phytochemicals of those mentioned above, which are used as reducing agents in the bioreduction of graphene oxide (GO) to form reduced graphene oxide (rGO). To illustrate the role of essential oils esters in reducing the GO to MERCF-rGO, a suggested mechanism with a high abundance in biosynthesis is shown in Fig. 9. The high percentage of

Table 2: GC-MS screening of the phytochemicals present in methanolic extract Iraqi *Rhus coriaria* (L.) fruits

No.	Retention time (min)	Area of peak (%)	Compound identified	Molecular formula	M.Wt (g/mol)	Structure
1	3.864	1.86	Acetic acid, hydroxy, ethyl ester	$C_4H_8O_3$	104.10	
2	4.758	0.83	Ethyl formate	$C_3H_6O_2$	74.08	
3	5.604	0.49	1-Propanol	C_3H_8O	60.1	
4	6.600	0.77	1,2-Benzendiol,3,5 bis(1,1dimethylethy)	$C_{14}H_{22}O_2$	222.3	
5	7.636	0.54	Gallic acid	$C_7H_6O_5$	170.12	
6	10.303	1.89	Caprolactam	$C_6H_{11}NO$	113.16	
7	12.588	0.71	3,5-Dimethyl-1dimethyl phenylsilyloxybenzene	$C_{16}H_{20}OSi$	256.41	
8	19.478	8.72	Hexadecanoic acid, methyl ester	$C_{17}H_{34}O_2$	270.45	
9	19.927	3.70	n-Hexadecanoic acid	$C_{16}H_{32}O$	256.43	
10	20.326	0.60	Metanephrine	$C_{10}H_{15}NO_3$	197.23	
11	21.466	14.58	9,12-Octadecadienoic acid, methyl ester	$C_{19}H_{34}O_2$	294.47	
12	21.550	19.76	9-Octadecenoic acid, methyl ester (E)	$C_{19}H_{36}O_2$	296.48	
13	21.628	7.81	11-Octadecenoic acid, methyl ester	$C_{19}H_{36}O_2$	296.49	
14	21.875	7.78	9,12-Octadecadienoic acid (Z,Z)	$C_{18}H_{32}O_2$	280.445	
15	22.02	15.63	cis-13-Octadecenoic acid	$C_{18}H_{34}O_2$	282.5	
16	22.257	3.69	cis-Vaccenic acid	$C_{18}H_{34}O_2$	282.5	
17	22.533	3.99	8,11- Octadecadienoic acid, methyl ester	$C_{19}H_{34}O_2$	294.47	
18	22.961	1.18	Isopropyl linoleate	$C_{21}H_{38}O_2$	322.5	
19	23.208	0.50	cis-11-Hexadecenal	$C_{16}H_{30}O$	238.41	
20	23.771	0.66	Oleic acid	$C_{18}H_{34}O_2$	282.468	
21	24.039	0.52	Eicosanoic acid, methyl ester	$C_{21}H_{42}O_2$	326.6	
22	24.879	1.55	Myricetin	$C_{15}H_{10}O_8$	318.24	
23	27.458	0.55	Cyclobarbital	$C_{12}H_{16}N_2O_3$	236.27	
24	27.709	0.85	1,2,5-Oxadiazol-3-amine, 4-(3-methoxyphenoxy)	$C_9H_9N_3O_3$	207.19	
25	29.709	0.86	Propiophenone-2' -(trimethyloxy)	$C_{12}H_{18}O_2Si$	222.35	

REDUCE GRAPHENE OXIDE NANOSHEETS DERIVED FROM IRAQI *RHHUS CORIARIA*(L.) FRUITS WERE EVALUATED FOR THEIR ANTICANCER AND ANTIBACTERIAL

PROPERTIES
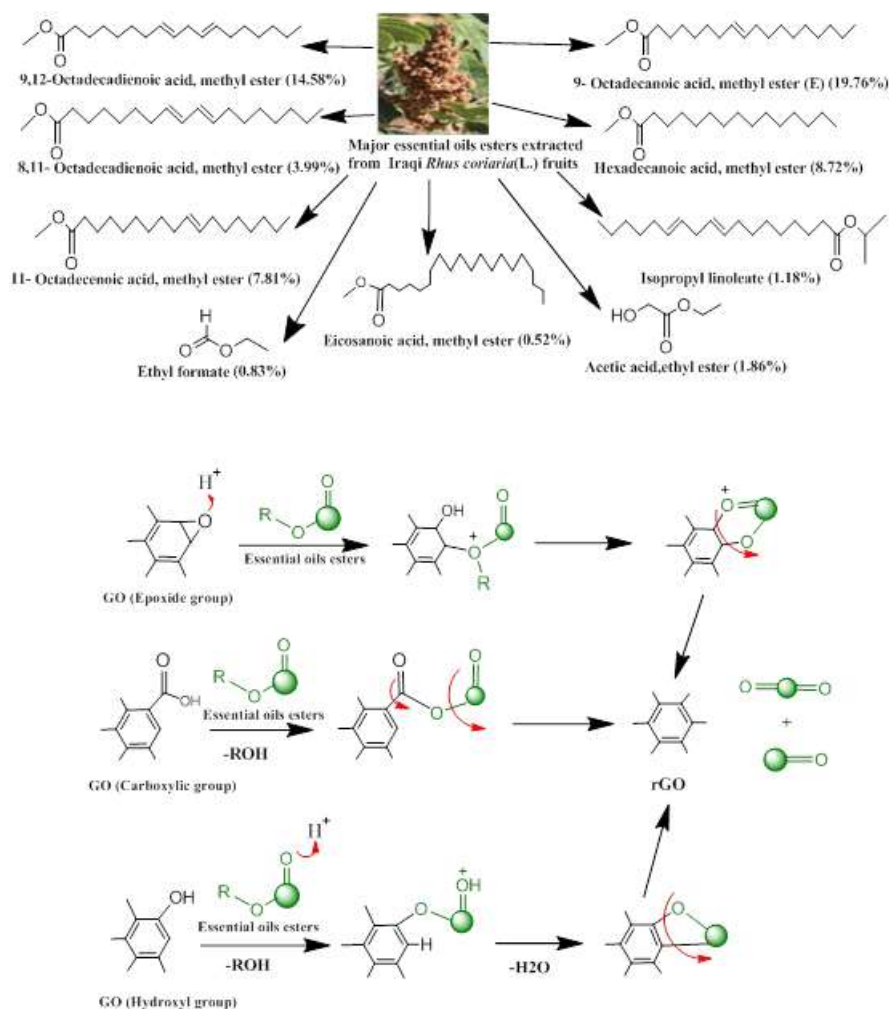
Figure 9: The suggested mechanism for the green synthesis of rGO using essential oils esters from methanolic extract of Iraqi *Rhus coriaria* (L.) fruits. Source: Elaborated by the authors.

these compounds in (MERCF) were 9-octadecanoic acid, methyl ester (E) followed by 9, 12-octadecanoic acid, methyl ester that is ($-COO-$) ester functional group. Graphene oxide (GO) includes adversity of functional groups on its surface like epoxy, carboxylic and hydroxyl groups. The epoxy group undergoes the ring's opening after the reaction with the essential oils esters. This represented the nucleophilic replacement that drives the formation new ring. After that, the ring splitting produced a double bond and removed the water molecule, which provides that GO is converted to rGO (Ansari *et al.*, 2019). Also, the hydroxyl group reacts with the essential oils esters that produce the new ring, followed by separating the ring to form rGO, the carboxylic group is subjected to the reaction condensation with the ester group to form a new ring and bond-producing to form rGO.

3.8. Antibacterial activity

The evolution of antimicrobial medicine is constantly challenging and expansive therefore, the nanomaterial (graphene materials) may be capable of turning off this hole to fight the antibiotic-resistant. Green synthesized rGO explained good antibacterial activity against both *S. aureus* (gram-positive) and *E. coli* (gram-negative) bacterial strains. The various concentrations of MERCF-rGO (15.62, 31.25, 62.5, 125) μg/mL explained the inhabitation zones diameters against *S. aureus* (12, 13, 17, 24 mm) and *E. coli* (13, 16, 19, 23 mm) respectively, as shown Fig. 10. The antibacterial activity of MERCF-rGO was compared with that of the commercial antibiotics (Augmentin, Ciprofloxacin, and Cefuroxime), the antibacterial activity of these antibiotics by using the concentration of (125 μg/mL) explained the inhabitation zone of the range of (8-12 mm) for both bacteria stain compare with the synthesized MERCF-rGO that confirmed this material antibacterial activity is higher from the commercial antibiotics. Also, this assay is taken the concentration of the commercial antibiotics (250 μg/mL) that is higher than the concentration of the prepared material MERCF-rGO (125 μg/mL), the antibacterial activity of MERCF-rGO is higher from the antibacterial activity of the commercial antibiotic (Augmentin, Cefuroxime, and Ciprofloxacin) that showed the inhabitation zone in the range of (9–14 mm) for both bacteria stain. It is significant that MERCF-rGO is a catchy antibacterial agent. The antibacterial effect of MERCF-rGO was increased with the increasing concentration for both types. The highest concentration (125 μg/mL) represented the highest antibacterial activity of MERCF-rGO. In the present study, the antibacterial activity of MERCF-rGO was investigated against *S. aureus* and *E. coli* , where the results displayed the dose-dependent manner. The antibacterial activity of MERCF-rGO is highest against *S. aureus* than *E.coli* due to the difference in the cell walls nature of bacteria as the structural chemistry of cell walls or the biological structure. Also, it is proposed that MERCF-rGO is connected with the bacteria, which possess the highest capacity to harm the membrane of bacteria cells, and it makes them porous, which leads the cell death (Zou *et al.*, 2014). The activity of inhibitor Iraqi *Rhus coriaria* (L.) fruits methanol extract depends on bacteria species and the extracted kind. The methanol extract of *Rhus coriaria* (L.) fruits is explained the antibacterial activity against the studied bacteria (Nostro *et al.*, 2016). Iraqi *Rhus coriaria* (L.) methanol extract is confirmed by GC/MS that is included essential oils as active constituents against microorganisms(Nasar–Abbas *et al.*, 2004).

3.9. MTT assay

This assay is carried out in vitro to know the cell viability of MERCF-rGO on human breast cancer cell lines (MCF-7). The effect of (MERCF-rGO) prepared on MCF-7 cells was dose-dependent with decreased cell viability and increased inhibition rate. The percent of cell viability was detected at 95.80 % to 60.81 % in (12.5 μg/mL to 200 μg/mL), respectively; as shown by the dose-dependent effect of MERCF-rGO, see Fig. 11. The IC$_{50}$ of MERCF-rGO was estimated at 251.99 μg/mL. The concentrations of MERCF-rGO (12.5 μg/mL, 25 μg/mL, 50 μg/mL, 100 μg/mL, 200 μg/mL) were used in the experiments. In this work, the anticancer efficacy of biosynthesized MERCF-rGO was assayed in vitro using a human breast cancer cell line (MCF-7) which showed the cell viability decreased with concentration. Many ways were followed
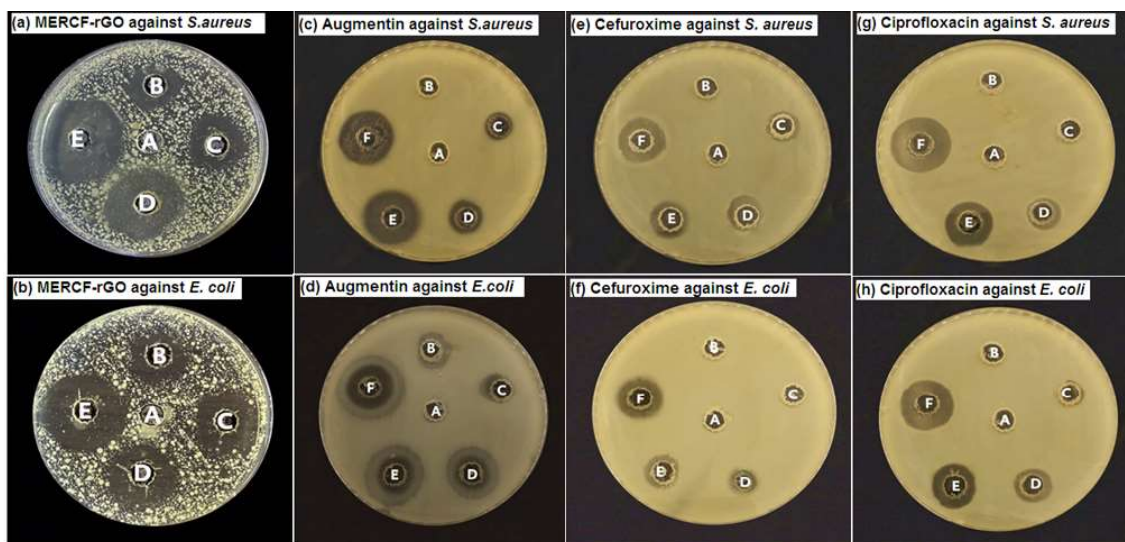
Figure 10: Inhibition zone image of MERCF-rGO and (positive control) Augmentin, Cefuroxime, and Ciprofloxacin (a), (b), (c), (d) against S. aureus and (e), (f), (g), (h) against *E. coli*

for the anticancer activity of reduced graphene oxide. Firstly, the graphene material like rGO interacts with the outer membrane of cancer cells (interact with the extracellular matrix and plasm membrane). Secondly, this material permeates the cell by binding to receptors spread and endocytosis (Rajivgandhi *et al.*, 2019). The functional properties of rGO are considered the basis for its toxicity. Therefore, the resulting reactive oxygen species occur after it's permeating the cell and which occur the little stress. The alternations of the cell cause the loss of functional features, and the inner organelles are harmed. When graphene material such as rGO arrives at the nucleus, and it might occur DNA harm, thus it causes to cell death (Tabish *et al.*, 2017). The reducing agent is an affected factor of the graphene materials' cytotoxicity (Singh *et al.*, 2012). In this study, the reducing agent was Iraqi *Rhus coriaria* (L.) fruits methanol extract and its bio components (such as essential oils ester, polyphenol etc.) attached to the reduced graphene oxide surface, thus the effects on the cell viability, which decreased with the concentration increasing therefore, MERCF-rGO considers as the powerful anticancer agent. Fig. 12 shows the morphological surface of the breast cancer cell MCF-7 (untreated cells) offers the landscape of accumulation as colonies. Conversely, shrinking and hiding numerous cells impacted by the MERCF-rGO cytotoxicity property.

3.10. Genotoxicity of MCF-7 fragmentation

The alkaline comet assay was used to investigate the MERCF-rGO capacity to damage the DNA of MCF-7 cells. The findings explain the DNA damage (depending on tail length) in MCF-7 for 48 h to IC_{50} concentration of MERCF-rGO (251.99 μg/mL), the genotoxic to MCF-7 cells depended on concentration and proportional with the rise to DNA fragmentation. Images of the microscope emphasized that treated cells had longer comet tail lengths conformable to the head, destroyed by treated cells, as shown in Fig. 13. Also, MERCF-rGO investigated the genotoxicity by comet assay for the known effect of MERCF-rGO on DNA
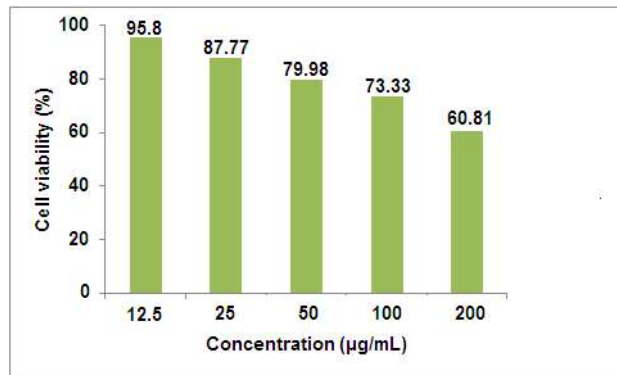
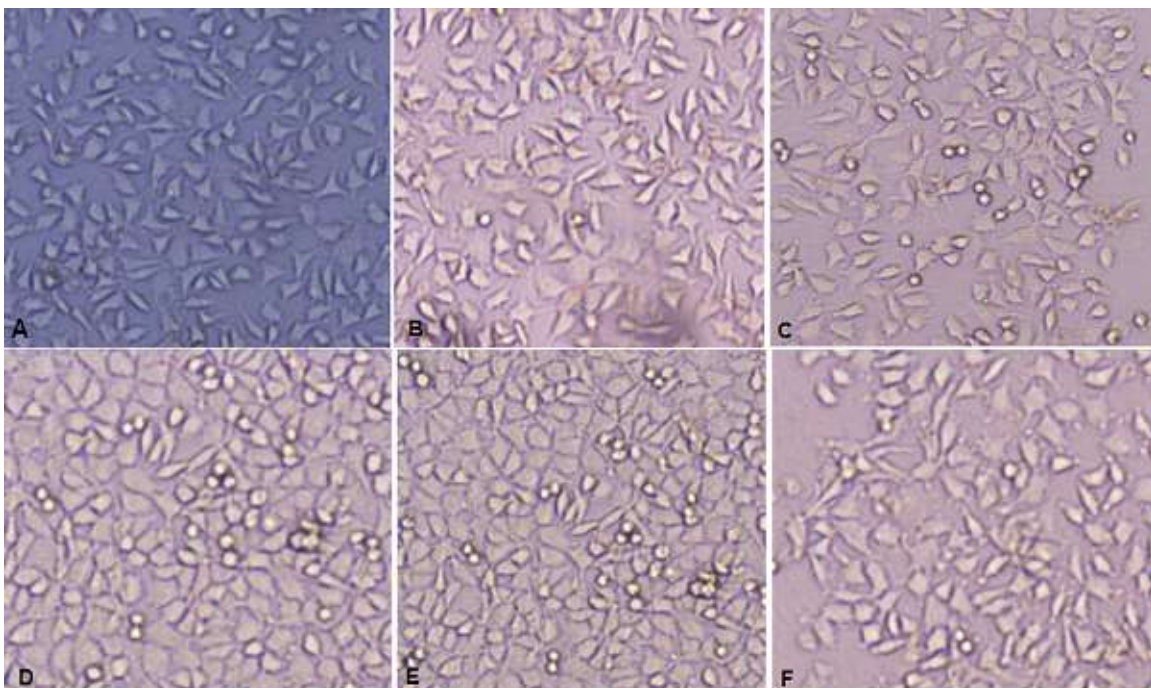Figure 11: Anticancer activity of MERCF-rGO at MCF-7.

Figure 12: Microscopic images of (A) untreated MCF-7 cells and (B, C, D, E, F) treated MCF-7 cells by different concentrations of MERCF-rGO (12.5, 25, 50, 100, 200) μg/mL.
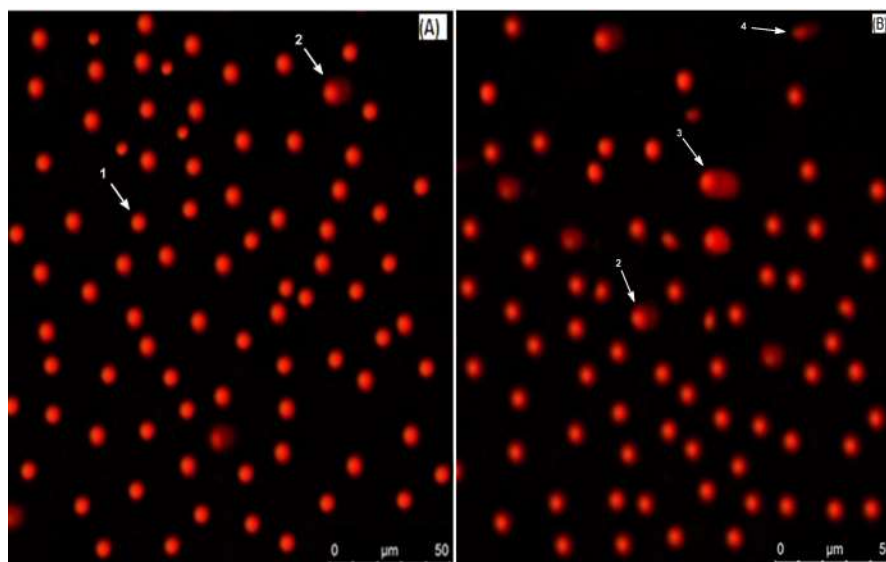
Figure 13: Effect of MERCF-rGO on DNA damage MCF-7 breast cancer cell line after 48 hr in (B) compared to control (A).

damage, where the results displayed the comet tail in the treated cell by MERCF-rGO compared with the control cell. rGO has hydrophobic natural and sharp edges; therefore, rGO penetrates cell components and interacts with DNA, causing genotoxicity effects (Jarosz *et al.*, 2016). When rGO enters the cell that induces intracellular generation, the reactive oxygen species (ROS) express the first step in the mechanisms of cancer. In addition (ROS) causes DNA fragmentation and mitochondria membrane disturbance that increases ROS generation followed by apoptosis. It is the phenomenon of the death cell (Domenech *et al.*, 2022).

4. CONCLUSIONS

Methanolic extract of Iraqi *Rhus coriaria* (L.) fruits acts as a reducing agent as a simple, cheap biosynthesis method resulting in *Rhus coriaria* (L.)-rGO nanosheets. Therefore, the reduction of GO by methanolic extract of Iraqi *Rhus coriaria* (L.) fruits was due to phytochemicals as essential oils and derivatives, polyphenols in the extract identified by GC/MS spectra. The GO and MERCF-rGO nanosheets have been used in various characterization studies as UV-Vis spectra at 226 and 238 nm, respectively. FTIR spectra determined the active groups in GO and MERCF-rGO, and XRD spectra of the GO and MERCF-rGO show the sizes at 10.42 and 4.07 nm, respectively. Further, FESEM of GO and MERCF-rGO explained the sheet shape for two samples. TEM shows a size lower than 10 nm for MERCF-rGO, whereas GO size is 15.54 nm. Also, the Raman spectra of GO and MERCF-rGO nanosheets showed two peaks D at ($1353 \, \text{cm}^{-1}$, $1336 \, \text{cm}^{-1}$ and G at ($1597 \, \text{cm}^{-1}$, $1594 \, \text{cm}^{-1}$, respectively. Afterwards, the characterization studies performed antibacterial activity of MERCF-rGO nanosheets that are known to be promoted by such bio-capping significantly verse gram-positive (*S. aureus*) than gram-negative (*E. coli*). The MTT assay shows that the prepared MERCF-rGO nanosheets also had anticancer features since they stopped cancer MCF-7 cells from growing. DNA

damage in comet assay suggested a possible role for ROS–induced DNA strand breaks. This work encourages for biosynthesis (green) rGO-based plants as promising, inexpensive, and having antimicrobial and anticancer activity.

Author's Contribution

Z. Al–Ali conceived and designed the study. She contributed to the writing and interpreting of the results of the manuscript.

A. Kadhim Biosynthesized and characterized the rGO and the bioapplications studies. She contributed to interpreting the results and writing the manuscript's initial draft. All authors participated in all manuscript requirements to produce a final version after being read and agreed upon by everyone.

Author's Declarations

Conflicts of interest: none.

We hereby confirm that all the figures in the manuscript are ours. Ethical Clearance: The authors declare that all experiments were done according to the ethical committee's permission from the University of Thi Qar.

References

Al-Abboodi, M. H., Ajeel, F. N. & Khudhair, A. M. (2017). Influence of oxygen impurities on the electronic properties of graphene nanoflakes. *Physica E: Low-dimensional Systems and Nanostructures*, 88, 1–5.

Alhwaige, A. A., Alhassan, S. M., Katsiotis, M. S., Ishida, H. & Qutubuddin, S. (2015). Interactions, morphology and thermal stability of graphene-oxide reinforced polymer aerogels derived from star-like telechelic aldehyde-terminal benzoxazine resin. *RSC advances*, 5(**112**), 92719–92731. doi:https://doi.org/10.1039/c5ra16188f.

Ansari, M. Z., Johari, R. & Siddiqi, W. A. (2019). Novel and green synthesis of chemically reduced graphene sheets using Phyllanthus emblica (Indian Gooseberry) and its photovoltaic activity. *Materials Research Express*, 6(**5**), 055027. doi:https://doi.org/10.1088/2053-1591/ab0439.

Aunkor, M., Mahbubul, I., Saidur, R. & Metselaar, H. (2015). Deoxygenation of graphene oxide using household baking soda as a reducing agent: a green approach. *RSC advances*, 5(**86**), 70461–70472. doi:https://doi.org/10.1039/c5ra10520j.

Bidan, A. K. & Al-Ali, Z. S. A. (2022). Biomedical Evaluation of Biosynthesized Silver Nanoparticles by Jasminum Sambac (L.) Aiton Against Breast Cancer Cell Line, and Both Bacterial Strains Colonies. *International Journal of Nanoscience*, 21(**06**), 2250042.

REDUCE GRAPHENE OXIDE NANOSHEETS DERIVED FROM IRAQI *RHHUS CORIARIA*(L.) FRUITS WERE EVALUATED FOR THEIR ANTICANCER AND ANTIBACTERIAL

PROPERTIES

Bidan, A. K. & Al-Ali, Z. S. A. (2023). Oleic and Palmitic Acids with Bioderivatives Essential Oils Synthesized of Spherical Gold Nanoparticles and Its Anti-Human Breast Carcinoma MCF-7 In Vitro Examination. *BioNanoScience*, 1–14.

Chandu, B., Mosali, V. S. S., Mullamuri, B. & Bollikolla, H. B. (2017). A facile green reduction of graphene oxide using Annona squamosa leaf extract. *Carbon letters*, 21, 74–80. doi:http://doi.org/10.5714/cl.2017.21.074.

Cheng, C., Li, S., Thomas, A., Kotov, N. A. & Haag, R. (2017). Functional graphene nanomaterials based architectures: biointeractions, fabrications, and emerging biological applications. *Chemical reviews*, 117(**3**), 1826–1914. doi:https://doi.org/10.1021/acs.chemrev.6b00520.

Choi, Y.-J., Gurunathan, S. & Kim, J.-H. (2018). Graphene oxide–silver nanocomposite enhances cytotoxic and apoptotic potential of salinomycin in human ovarian cancer stem cells (OvCSCs): A novel approach for cancer therapy. *International Journal of Molecular Sciences*, 19(**3**), 710. doi:https://doi.org/10.3390/ijms19030710.

Chu, H.-J., Lee, C.-Y. & Tai, N.-H. (2014). Green reduction of graphene oxide by Hibiscus sabdariffa L. to fabricate flexible graphene electrode. *Carbon*, 80, 725–733. doi:http://doi.org/10.1016/j.carbon.2014.09.019.

Domenech, J., Rodríguez-Garraus, A., López de Cerain, A., Azqueta, A. & Catalán, J. (2022). Genotoxicity of Graphene-Based Materials. *Nanomaterials*, 12(**11**), 1795. doi:https://doi.org/10.3390/nano12111795.

Emiru, T. F. & Ayele, D. W. (2017). Controlled synthesis, characterization and reduction of graphene oxide: A convenient method for large scale production. *Egyptian Journal of Basic and Applied Sciences*, 4(**1**), 74–79. doi:https://doi.org/10.1016/j.ejbas.2016.11.002.

Giovanelli, S., Giusti, G., Cioni, P. L., Minissale, P., Ciccarelli, D. & Pistelli, L. (2017). Aroma profile and essential oil composition of Rhus coriaria fruits from four Sicilian sites of collection. *Industrial Crops and Products*, 97, 166–174. doi:http://doi.org/10.1016/j.indcrop.2016.12.018.

Haghighi, B. & Tabrizi, M. A. (2013). Green-synthesis of reduced graphene oxide nanosheets using rose water and a survey on their characteristics and applications. *RSC advances*, 3(**32**), 13365–13371. doi: https://doi.org/10.1039/c3ra40856f.

Hinzmann, M., Jaworski, S., Kutwin, M., Jagiełło, J., Koziński, R., Wierzbicki, M., Grodzik, M., Lipińska, L., Sawosz, E. & Chwalibog, A. (2014). Nanoparticles containing allotropes of carbon have genotoxic effects on glioblastomamultiforme cells. *International journal of nanomedicine*, 9, 2409. doi:https://doi.org/10.2147/ijn.s62497.

Jarosz, A., Skoda, M., Dudek, I. & Szukiewicz, D. (2016). Oxidative stress and mitochondrial activation as the main mechanisms underlying graphene toxicity against human cancer cells. *Oxidative Medicine and Cellular Longevity*, 2016. doi:https://doi.org/10.1155/2016/5851035.

Jiříčková, A., Jankovský, O., Sofer, Z. & Sedmidubský, D. (2022). Synthesis and applications of graphene oxide. *Materials*, 15(**3**), 920. doi:https://doi.org/10.3390/ma15030920.

Khan, M., Al-Marri, A. H., Khan, M., Shaik, M. R., Mohri, N., Adil, S. F., Kuniyil, M., Alkhathlan, H. Z., Al-Warthan, A. & Tremel, W. (2015). Green approach for the effective reduction of graphene oxide using Salvadora persica L. root (Miswak) extract. *Nanoscale research letters*, 10(**1**), 1–9. doi:http://doi.org/10.1186/s11671-015-0987-z.

Kim, S.-G., Park, O.-K., Lee, J. H. & Ku, B.-C. (2013). Layer-by-layer assembled graphene oxide films and barrier properties of thermally reduced graphene oxide membranes. *Carbon letters*, 14(**4**), 247–250. doi:https://doi.org/10.5714/cl.2013.14.4.247.

Lin, S., Ruan, J. & Wang, S. (2019). Biosynthesized of reduced graphene oxide nanosheets and its loading with paclitaxel for their anti cancer effect for treatment of lung cancer. *Journal of Photochemistry and Photobiology B: Biology*, 191, 13–17.

Lingaraju, K., Naika, H. R., Nagaraju, G. & Nagabhushana, H. (2019). Biocompatible synthesis of reduced graphene oxide from Euphorbia heterophylla (L.) and their in-vitro cytotoxicity against human cancer cell lines. *Biotechnology Reports*, 24, e00376. doi:http://doi.org/10.1016/j.btre.2019.e00376.

Ma, N., Zhang, B., Liu, J., Zhang, P., Li, Z. & Luan, Y. (2015). Green fabricated reduced graphene oxide: evaluation of its application as nano-carrier for pH-sensitive drug delivery. *International Journal of Pharmaceutics*, 496(**2**), 984–992.

Mahendran, R., Sridharan, D., Santhakumar, K., Selvakumar, T., Rajasekar, P. & Jang, J.-H. (2016). Graphene oxide reinforced polycarbonate nanocomposite films with antibacterial properties. *Indian Journal of Materials Science*, 2016. doi:https://doi.org/10.1155/2016/4169409.

Mahmoud, A. E. D. (2020). Eco-friendly reduction of graphene oxide via agricultural by-products or aquatic macrophytes. *Materials Chemistry and Physics*, 253, 123336. doi:https://doi.org/10.1016/j.matchemphys.2020.123336.

Marcano, D. C., Kosynkin, D. V., Berlin, J. M., Sinitskii, A., Sun, Z., Slesarev, A., Alemany, L. B., Lu, W. & Tour, J. M. (2010). Improved synthesis of graphene oxide. *ACS nano*, 4(**8**), 4806–4814. doi:https://doi.org/10.1021/nn1006368.

Mazaheri, T., Hesarinejad, M., Razavi, S., Mohammadian, R. & Poorkian, S. (2017). Comparing physicochemical properties and antioxidant potential of sumac from Iran and turkey. *MOJ Food Process Technol*, 5(**2**), 288–294. doi:https://doi.org/10.15406/mojfpt.2017.05.00125.

Muthoosamy, K., Abubakar, I. B., Bai, R. G., Loh, H.-S., & Manickam, S. (2016). Exceedingly higher co–loading of curcumin and paclitaxel onto polymer-functionalized reduced graphene oxide for highly potent synergistic anticancer treatment. *Scientific reports*, 6(**1**), 32808.

Nasar–Abbas, S., Halkman, A. K., & Al–Haq, M. (2004). Inhibition of some foodborne bacteria by alcohol extract of sumac (Rhus coriaria L.). *Journal of food safety*, 24(**4**), 257–267. doi:https://doi.org/10.1111/j.1745-4565.2004.00506.x.

Nostro, A., Guerrini, A., Marino, A., Tacchini, M., Di Giulio, M., Grandini, A., Akin, M., Cellini, L., Bisignano, G. & Saraçoğlu, H. T. (2016). In vitro activity of plant extracts against biofilm-producing food-related bacteria. *International Journal of Food Microbiology*, 238, 33–39. doi:https://doi.org/10.1016/j.ijfoodmicro.2016.08.024.

Olumurewa, K. O., Olofinjana, B., Fasakin, O., Eleruja, M. A. & Ajayi, E. O. B. (2017). Characterization of high yield graphene oxide synthesized by simplified hummers method. *Graphene*, 6(**4**), 85–98. doi:https://doi.org/10.4236/graphene.2017.64007.

Punniyakotti, P., Aruliah, R. & Angaiah, S. (2021). Facile synthesis of reduced graphene oxide using Acalypha indica and Raphanus sativus extracts and their in vitro cytotoxicity activity against human breast (MCF-7) and lung (A549) cancer cell lines. *3 Biotech*, 11(**4**), 1–11. doi:https://doi.org/10.1007/s13205-021-02689-9.

Rajivgandhi, G., Maruthupandy, M., Quero, F. & Li, W.-J. (2019). Graphene/nickel oxide nanocomposites against isolated ESBL producing bacteria and A549 cancer cells. *Materials Science and Engineering: C*, 102, 829–843. doi:https://doi.org/10.1016/j.msec.2019.05.008.

Rani, M. N., Ananda, S. & Rangappa, D. (2017). Preparation of reduced graphene oxide and its antibacterial properties. *Materials Today: Proceedings*, 4(**11**), 12300–12305. doi:https://doi.org/10.1016/j.matpr.2017.09.163.

Rochman, R. A., Wahyuningsih, S., Ramelan, A. H. & Hanif, Q. A. (2019). *Preparation of nitrogen and sulphur Co-doped reduced graphene oxide (rGO-NS) using N and S heteroatom of thiourea.* Paper presented at the IOP Conference Series: Materials Science and Engineering.

Singh, S. K., Singh, M. K., Kulkarni, P. P., Sonkar, V. K., Grácio, J. J. & Dash, D. (2012). Amine-modified graphene: thrombo-protective safer alternative to graphene oxide for biomedical applications.*ACS nano*, 6(**3**), 2731–2740. doi:https://doi.org/10.1021/nn300172t.

Tabish, T. A., Pranjol, M. Z. I., Hayat, H., Rahat, A. A., Abdullah, T. M., Whatmore, J. L. & Zhang, S. (2017). In vitro toxic effects of reduced graphene oxide nanosheets on lung cancer cells. *Nanotechnology*, 28(**50**), 504001. doi:https://doi.org/10.1088/1361-6528/aa95a8.

Thiyagarajulu, N., Arumugam, S., Narayanan, A. L., Mathivanan, T. & Renuka, R. R. (2020). Green synthesis of reduced graphene nanosheets using leaf extract of tridax procumbens and its potential in vitro biological activities. *Biointerface Res. Appl. Chem*, 11, 9975–9984.

Wu, C., Wu, X., Yang, Y., Zhou, X. & Wu, H. (2012). Biological Applications of Graphene and Graphene Oxide. *Nano Biomedicine & Engineering*, 4(**3**).

Yi, J., Choe, G., Park, J. & Lee, J. Y. (2020). Graphene oxide-incorporated hydrogels for biomedical applications. *Polymer Journal*, 52(**8**), 823–837.

Zhu, C., Guo, S., Fang, Y. & Dong, S. (2010). Reducing sugar: new functional molecules for the green synthesis of graphene nanosheets. *ACS nano*, 4(**4**), 2429–2437.

Zou, X., Zhang, L., Wang, Z. & Luo, Y. (2016). Mechanisms of the antimicrobial activities of graphene materials. *Journal of the american chemical society*, 138(**7**), 2064–2077. doi:https://doi.org/10.1021/jacs.5b11411.